# Spatiotemporal Structure of H$\alpha$ Emission from the Detached Plasma in GAMMA 10/PDX*)

Hirohiko TANAKA, Mizuki SAKAMOTO[1)], Naomichi EZUMI[1)], Akihiro TERAKADO[1)], Kunpei NOJIRI[1)], Tomohiro MIKAMI[1)], Yosuke KINOSHITA[1)], Kaede KOBAYASHI[1)], Masayuki YOSHIKAWA[1)], Junko KOHAGURA[1)] and Noriyasu OHNO

*Graduate School of Engineering, Nagoya University, Chikusa-ku, Nagoya 464-8603, Japan*
[1)]*Plasma Research Center, University of Tsukuba, 1-1-1 Tennodai, Tsukuba 305-8577, Japan*

(Received 6 September 2018 / Accepted 10 January 2019)

High-speed camera measurement was performed for analyses of detached plasma fluctuation in the GAMMA 10/PDX tandem mirror device. Significant spectral peaks at frequencies of 1.5 and 3 kHz were observed to have several local maxima along the vertical, near the entrance of the V-shaped target. Wavelet analysis indicated that 1.5- and 3-kHz fluctuations became non-simultaneously strong. Their phase relationships demonstrated inversion-symmetric and symmetric features with respect to the midplane. Such spectral patterns were interpreted as the line-integral of odd- and even-mode structures. It is suspected that the vertical edge part was due to radially elongated structures with an azimuthal phase shift.



Keywords: fluctuation, plasma detachment, high-speed camera, frequency analysis, GAMMA 10/PDX

DOI: 10.1585/pfr.14.2402036

## 1. Introduction

Plasma detachment is sought so as to achieve a sufficient reduction in divertor heat load by promoting radiation and recombination processes via plasma-neutral gas interactions. Recently, enhanced non-diffusive transport that broadens the plasma profile across the magnetic field was observed under the detached divertor condition in several magnetic confinement devices [1–3]. As the profile broadening contributes to the peak-flux reduction in addition to the conventional detachment theory, our understanding of the transport mechanism becomes more valuable.

For the GAMMA 10/PDX tandem mirror device, a recent study shows that blob-/hole-like isolated high-/low-density structures appeared at the radial outer-side edge inside the "divertor simulation experimental module (D-module)" [4]. By using Langmuir probes in the D-module and upstream microwave interferometers, it was observed that blob-/hole-like structures were outstanding during the transient state between the attached and detached divertor states. Further, these structures rotated in the azimuthal direction together with the rotation of a few mode-number structures. In this previous research, although multipoint fluctuation characteristics were clarified with intrinsic high spatial resolution of Langmuir probes, dependencies in radial and axial directions cannot be separately discussed due to the structure arrangement.

The high-speed camera is an effective solution for measuring wide-range fluctuation without any disturbance in observed plasma parameters. In this study, we applied a high-speed camera viewing inside the D-module and first investigated the fluctuation characteristics of the detached plasma emission in GAMMA 10/PDX. Fourier and wavelet analyses demonstrated vertical locations of several anomalous spectral peaks that were attributed to the line-integral effect. To interpret the obtained frequency characteristics, synthetic data based on a simplified model was generated and compared.

In Sec. 2, experimental setup is described. In Sec. 3, frequency analysis is presented and compared with synthetic patterns. Finally, in Sec. 4, we discuss our experimental results and summarize our study.

## 2. Experimental Setup

GAMMA 10/PDX equips the D-module in the west-end cell with a divergent magnetic field, to study divertor physics [5]. To evaluate the divertor plasma characteristics, there are several measurement systems inside the D-module, e.g., Langmuir probes, a spectrometer, and a high-speed camera [6].

Figure 1 shows a snapshot of 2D images on the $x$-$z$ plane viewed from the north side of the D-module. In this study, a movie data of the H$\alpha$ emission intensity, $I_{\mathrm{H}\alpha}$, which is proportional to the product of neutral and electron densities, was obtained using an optical filter. The frame rate and shutter speed were 20 kHz and 10 µs, respectively. Although this frame rate was insufficient for detecting blob- and hole-like structures [4], the measured region covered a wide area inside the D-module and mode

*author's e-mail: h-tanaka@ees.nagoya-u.ac.jp*

*) This article is based on the presentation at the 12th International Conference on Open Magnetic Systems for Plasma Confinement (OS2018).

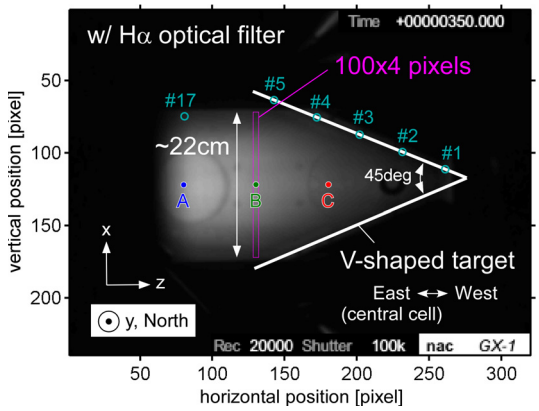


Fig. 1 Snapshot of Hα emission movie at $t = 350$ ms with the V-shaped target and Langmuir probes.

structures at several kilohertz could be captured. The amplitude resolution was 8 bits (256 tonal values for each pixel) and the frame size was $240 \times 320$ pixels. The approximate position of the V-shaped target with Langmuir probes (#1 - #5) is also depicted in Fig. 1. The inner angle of the V-shaped target was set to 45°. At the same time, probe #17 was located almost upstream of probe #5 along the magnetic field with a slight deviation in the azimuthal direction. Ion saturation current ($I_{sat}$) fluctuations were acquired at a sampling frequency of 500 kHz.

In this study, we mainly analyzed $I_{H\alpha}$ fluctuations inside the vertically elongated rectangle area ($100 \times 4$ pixels) near the entrance of the V-shaped target, which avoids the non-uniform reflection from backstructures such as a flange and bolt holes (see Fig. 1). To reduce noise and increase amplitude resolution, $I_{H\alpha}$ was averaged at $4 \times 4$ pixels, which corresponds to an $\sim 8.8 \times 8.8$ mm$^2$ area on the $x$-$z$ plane, in the undermentioned analyses. Thus, 25 sets of time-series data resized from the rectangular $100 \times 4$ pixels will be investigated below.

# 3. Measurement and Analysis

A transient discharge from the attached to detached states was analyzed (shot number: 243740). Plasma was sustained with the ion cyclotron range of frequency waves. This discharge is the same as that in the previous study [4] where the high-speed camera data had not yet been analyzed.

## 3.1 Time series in the transient discharge

Figure 2 shows the time series of the diamagnetism ($DM_{CC}$), the electron line density ($NL_{CC}$) in the central cell, $I_{sat}$ at probes #1, #5, and #17, and $I_{H\alpha}$ at three different $z$ positions (A, B, and C) at $x \sim 0$ (see Fig. 1). In this discharge, $H_2$ gas was puffed with a plenum pressure of 800 mbar in the middle of a 400-ms pulse discharge. From $t \sim 150$ ms, $I_{sat}$ and $I_{H\alpha}$ increase due to the gas injection. A little later, $DM_{CC}$ and $NL_{CC}$ start to get affected slightly.

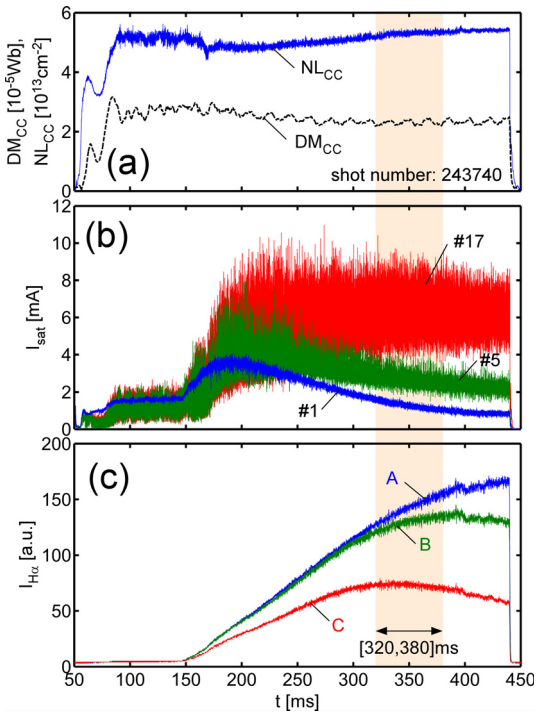


Fig. 2 Time series of (a) $DM_{CC}$ (dashed line), $NL_{CC}$ (solid line), (b) $I_{sat}$ at probes #1, #5, and #17, and (c) raw $I_{H\alpha}$ at three positions (A, B, and C in Fig. 1).

On the V-shaped target, we can observe the rollover of $I_{sat}$ after $t \sim 200$ ms. This results from plasma detachment. At $t > \sim 300$ ms, the decreasing and increasing tendencies of $I_{sat}$ and $I_{H\alpha}$, respectively, weaken.

Hereafter, a quasi-steady-state detached period with large-amplitude $I_{H\alpha}$ at the entrance of the V-shaped target ($t = [320, 380]$ ms) will be investigated in detail.

## 3.2 Frequency characteristics

Figure 3 (a) shows the Fourier power spectra of $I_{H\alpha}$ as functions of the frequency, $f$, and $x$, demonstrating a seemingly strange pattern. There are spectral peaks at $f \sim 1.5$ and 3 kHz with different $x$ locations. In addition, a smaller-amplitude peak is confirmed at 4.5 kHz. Figure 3 (b) shows the vertical distribution of the standard deviation ($\sigma$) of $I_{H\alpha 1}$, $I_{H\alpha 2}$, and $I_{H\alpha 3}$. Here, $I_{H\alpha 1}$, $I_{H\alpha 2}$, and $I_{H\alpha 3}$ are defined as the band-passed signals of $I_{H\alpha}$ at $f_1 = [1, 2]$ kHz, $f_2 = [2.5, 3.5]$ kHz, and $f_3 = [4, 5]$ kHz, respectively. The standard deviations of $I_{H\alpha 1}$ and $I_{H\alpha 3}$ have a local minimum at $x = 0$, while $\sigma$ of $I_{H\alpha 2}$ has a local maximum at the same position. It should be noted that these distributions have 4 - 5 local maxima along $x$ with large amplitudes near the center and small amplitudes at the edge.

To detect appearances of these periodic fluctuations in time, the wavelet transform was applied with the Morlet mother wavelet [7]. Figures 3 (c) and (d) show the absolute values of the wavelet coefficients at $f = 1.5$ and 3 kHz, respectively, as functions of $t$ and $x$. The former

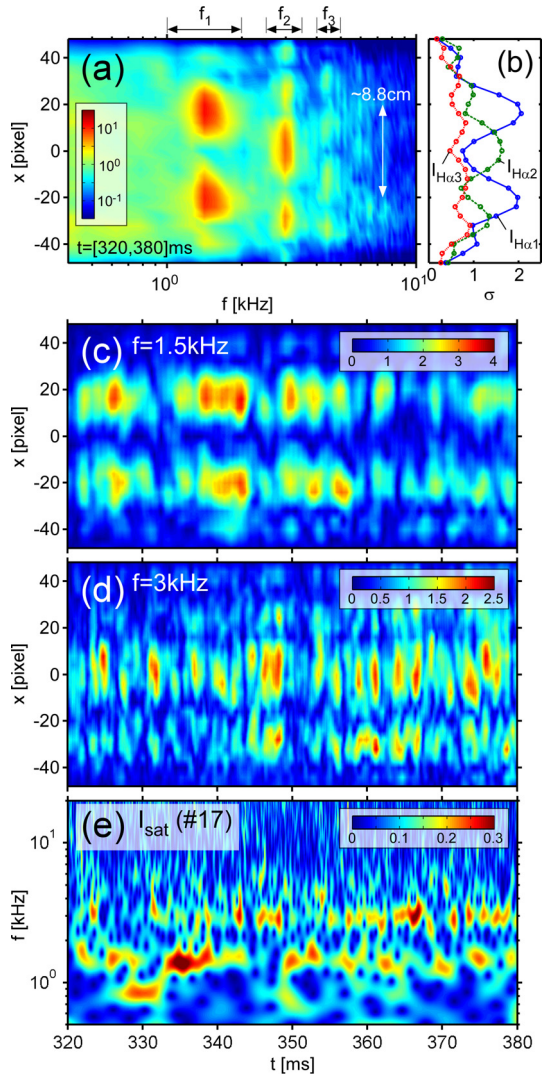


Fig. 3 (a) Fourier power spectra of $I_{H\alpha}$ at $t = [320, 380]$ ms as functions of $f$ and $x$. (b) $\sigma$ of $I_{H\alpha1}$ (solid line), $I_{H\alpha2}$ (dashed line), and $I_{H\alpha3}$ (dotted line) along $x$. The absolute values of the wavelet coefficients of (c) $I_{H\alpha}$ at 1.5 kHz and (d) 3 kHz as functions of $t$ and $x$, and (e) $I_{sat}$ at probe #17 as functions of $t$ and $f$.

fluctuation seems to appear frequently at $t < \sim 360$ ms. On the contrary, the latter fluctuation largely occurs at $t > \sim 345$ ms. These fluctuations are thought to be strong non-simultaneously. Figure 3 (e) shows the absolute value of the wavelet coefficient of $I_{sat}$ at probe #17 versus $t$ and $f$. Amplitudes of $f = 1.5$ and 3 kHz components in the $I_{sat}$ fluctuation show similar temporal tendencies with those of $I_{H\alpha}$.

### 3.3 Phase relationship along the $x$ direction

To interpret the periodic fluctuations shown in Fig. 3, the spatiotemporal behavior of the phase relationship was investigated. Figures 4 (a) and (b) show fluctuation components $(I_{H\alpha} - \langle I_{H\alpha}\rangle_m)$ as functions of $t$ and $x$ at $t = [337, 339]$ ms and $[363, 365]$ ms. In the former period, the 1.5-kHz fluctuation is dominant, whereas the 3-kHz component is strong in the latter period, as shown in Fig. 3 (e). Here, $\langle I_{H\alpha}\rangle_m$ means the simple moving average of $I_{H\alpha}$ over 200 points (10 ms), mainly consisting of low-frequency components at $f < 100$ Hz. These figures show wire-mesh like features with different inclined angles around the mid-plane.

Figures 4 (c)(d) and (e)(f) show $I_{H\alpha1}$ and $I_{H\alpha2}$, respectively. It can be confirmed that $I_{H\alpha1}$ in the former and $I_{H\alpha2}$ in the latter periods are strong. From Fig. 4 (c), $I_{H\alpha1}$ at $x \sim +18$ and $-18$ pixels are observed to be anti-phase. Further, $I_{H\alpha1}$ at $x \sim \pm 18$ pixels seem to be anti-phase to $I_{H\alpha1}$ at $x \sim \pm 40$ pixels. On the contrary, $I_{H\alpha2}$ at $x \sim 0$ and $\pm 28$ pixels are anti-phase, and $I_{H\alpha2}$ at $x \sim \pm 28$ and $\pm 44$ pixels are anti-phase.

Considering the line-integral effect of the high-speed camera measurement, odd- and even-mode structures should become weak and strong at $x = 0$, respectively. Therefore, fluctuations at 1.5 and 3 kHz must be attributed to odd and even modes, respectively. This presumption agrees with the supposition from the microwave interferometer and the segmented central limiter measurements in the previous study [4] where the azimuthal mode numbers ($m$) of 1.5- and 3-kHz fluctuations were supposed to be $m = 1$ and 2, respectively.

### 3.4 Synthetic patterns based on a simplified model

To understand detailed mode structures, we generated a similar plot from a simplified artificial mode function considering the line-integral effect. Figure 5 shows the synthetic patterns calculated from the modeled signals as functions of $t$ and $x$. In this calculation, we assumed that a mode has an amplitude with $\sin(2\pi m f_{rot} t - m\theta)$, where $\theta$ is the azimuthal angle, existing on a single circle with radius $R_0$, and it rotates with a frequency of $f_{rot}$. At an $x$-position where the mode intensities at forward and back sides in the line of sight are in-phase/anti-phase, $I_{H\alpha}$ becomes strong/weak. In addition, $I_{H\alpha}$ at $|x| \sim R_0$ becomes strong due to the line-integral of a self-structure.

Mode structures at $m = 1$ and $m = 2$ rotating with $f_{rot} = 1.5$ kHz could reproduce the experimentally observed phase relationships around $x = 0$, as shown in Figs. 5 (a) and (b). However, in the far-edge region at $|x| > R_0$, there is no structure unlike Figs. 4 (c) and (f). To obtain the far-edge structures with a single mode on a circle, $m = 3$ and 4 were employed, as shown in Figs. 5 (c) and (d). When higher-order modes are used, experimentally observed inclined angles of in-phase region around $x = 0$ can be obtained when $f_{rot} = 0.5$ kHz for $m = 3$ and $f_{rot} = 0.75$ kHz for $m = 4$. Although center- and edge-phase relationships are reproduced, an alternate appearance of $m = 3$ and 4 structures of varying rotational frequencies is unnatural.

One of the possible reasons that the far-edge structures cannot be reconstructed from $m = 1$ and 2 modes in the

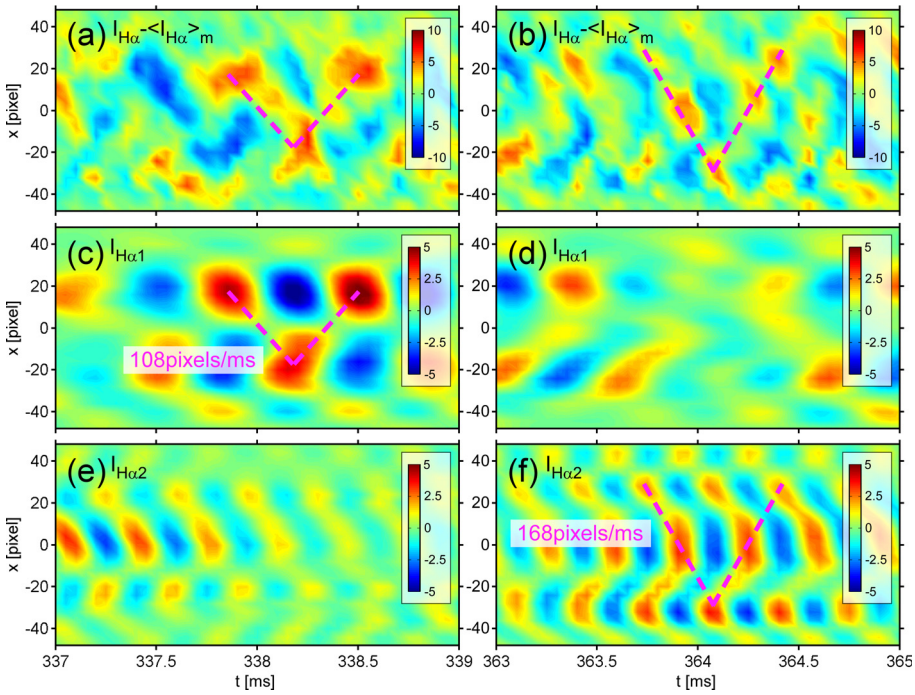


Fig. 4 (a)(b) $I_{H\alpha} - \langle I_{H\alpha}\rangle_m$, (c)(d) $I_{H\alpha1}$, and (e)(f) $I_{H\alpha2}$ as functions of $t$ and $x$ at (a)(c)(e) $t = [337, 339]$ ms and (b)(d)(f) [363, 365] ms.

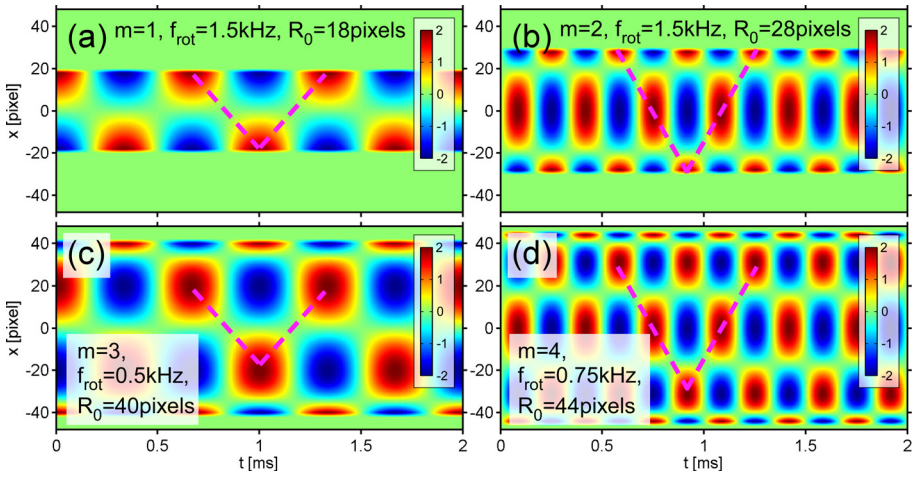


Fig. 5 Synthetic patterns from modeled signals with (a) $m = 1$, (b) 2, (c) 3, and (d) 4. $f_{rot}$ was calculated as the peak frequency divided by $m$. $R_0$ was determined from the peak position of $\sigma$ in Fig. 3 (b).

above calculation is attributed to the assumption that the mode exists on a single circle. A mode structure should have a finite size and it could have an azimuthal phase shift in the radial direction. For example, if a mode structure had a spiral shape like Refs. [8,9], the phase relationship could have an anti-phase structure in the far-edge region.

## 4. Summary and Discussion

High-speed camera measurement of the detached plasma fluctuation was performed using GAMMA 10/PDX. To investigate spatiotemporal patterns of the mode structures, Fourier and wavelet transforms were applied. In addition, band-passed signals were plotted to understand the phase relationship in the vertical direction. It was clarified that odd- and even-mode structures were detected as the spectral peaks at $f = 1.5$ and 3 kHz. If their rotation frequencies were the same, azimuthal mode numbers were $m = 1$ and 2. However, it was also observed that a low-$m$ structure on a single circle cannot reproduce the experimentally observed far-edge phase pattern. There might be radially elongated structures with an azimuthal phase shift. To clarify the shapes of the mode structures, a comparison between the emission signals and other fluctu-

ations that have no line-integral effect would be effective. We are now planning to use a reciprocating probe just in front of the D-module in addition to the high-speed camera and Langmuir probes on the V-shaped target.

Because the blob- and hole-like structures reported in Ref. [4] lay in the $f > 10$-kHz frequency range and the Nyquist frequency of the above-described high-speed camera measurement was 10 kHz, we could not detect these structures in this study. In future, we should capture with higher temporal resolution. Furthermore, the instability type should be clarified with the radial electric field measurement, among others.

## Acknowledgments

This research was supported by JSPS KAKENHI (16H06139, 16H02440), the NIFS Collaboration Research program (NIFS17KUGM120, NIFS17KUGM130), and the NINS program of Promoting Research by Networking among Institutions (01411702).

[1] H. Tanaka *et al.*, Phys. Plasmas **17**, 102509 (2010).
[2] D. Carralero *et al.*, Nucl. Fusion **58**, 096015 (2018).
[3] H. Tanaka *et al.*, Plasma Phys. Control. Fusion **60**, 075013 (2018).
[4] H. Tanaka *et al.*, Phys. Plasmas **25**, 082505 (2018).
[5] Y. Nakashima *et al.*, Nucl. Fusion **57**, 116033 (2017).
[6] A. Terakado *et al.*, AIP Conf. Proc. **1771**, 050008 (2016).
[7] N. Ohno *et al.*, Contrib. Plasma Phys. **44**, 222 (2004).
[8] S. Inagaki *et al.*, Nucl. Fusion **52**, 023022 (2012).
[9] H. Tanaka *et al.*, Contrib. Plasma Phys. **50**, 256 (2010).